

Resource-Constrained Busbar Sizing: Evaluating the Impact of Insulator Geometry and Pattern

E. Appolinaire Dantondji^{1,2}, Edith Clavel¹, James Roudet¹, Jean-Michel Guichon¹, Alexis Derbey¹, Etienne Gautron²

¹Univ. Grenoble Alpes, CNRS, Grenoble INP, G2Elab, 38000 Grenoble, France,
enagnon-appolinaire.dantondji@g2elab.grenoble-inp.fr

²Gindre Duchavany, Gindre Composants, F-38230, Pont-de-Chérury, France,
gautron.e@gindre.com

Executive Summary

In resource-constrained electrical systems, optimizing busbar thermal and material performance is critical. This study uses a fast and efficient hybrid electrothermal modeling approach, coupling the Partial Element Equivalent Circuit (PEEC) method with thermal energy balance equations, to evaluate how insulation properties, surface treatments, and geometric patterning impact busbar behavior. Results show that applying sawtooth patterns to the insulator surface increases effective heat dissipation without altering the main physical dimensions, reducing copper temperatures by up to 24% compared to traditional flat configurations. Surface treatments enhancing emissivity also deliver significant thermal benefits. Experimental validation demonstrates strong agreement with simulations, highlighting potential material savings of 20 to 41% while preserving safety and electrical standards. The proposed design strategies provide engineers with practical tools to build more compact, efficient, and reliable busbar systems, supporting smarter industrial and infrastructure applications where space, thermal performance, and material optimization are increasingly decisive.

Keywords: Materials for Evs, Energy storage systems, Thermal management, Sustainable Energy, Modelling & Simulation

1 Introduction

The growing demand for compact, efficient, and sustainable electrical systems is driving the need for innovative busbar designs that balance thermal performance, material efficiency, safety standards and system reliability. Busbars, as critical current-carrying components, pose complex optimization challenges: while resistive losses generate heat that accelerates material aging, simply increasing the copper cross-section conflicts with sustainability, compactness, and weight constraints — particularly in mobile applications. In thermally constrained systems, enhancing surface heat dissipation becomes a key strategy to control conductor temperature without enlarging either its size or its mass. As high currents produce significant Joule heating, improving convective and radiative cooling at the busbar surface is essential to maintain thermal balance and ensure long-term reliability. Traditional busbar sizing methods often prioritize conservative safety margins, often leading to oversizing and inefficient material usage. Even recent design approaches relying on finite element methods (FEM) struggle to balance computational efficiency with the multiphysics complexity of coupled electromagnetic-thermal phenomena [1]. However, advances in system optimization now emphasize the need for smarter, more resource-conscious approaches. In this context, optimizing thermal management has emerged as a key enabler for material savings and system miniaturization. Surface treatments, improved insulation properties, and geometric modifications such as patterned surfaces offer promising solutions to enhance heat dissipation without increasing the physical size of conductors [2]. Studies demonstrate that emissivity-enhancing treatments can significantly increase busbar ampacity at

equivalent temperatures [3], while textured surfaces improve convective cooling through turbulent airflow induction. However, existing research lacks systematic evaluation of how combined insulator geometry modifications and surface treatments interact with electromagnetic constraints – a gap this study addresses through hybrid electrothermal modeling approaches, combining circuit-based electromagnetic models with detailed thermal energy balance equations, provide high-fidelity solutions means to analyze the complex interactions between electrical and thermal behaviors. Coupled with thermal energy balance equations, these hybrid methods allow rapid parametric evaluations of design variations, facilitating practical decision-making at early design stages. These methods allow designers to explore a wide range of material and geometric configurations with minimal computational burden.

This study investigates how insulation thermal conductivity, thickness, surface emissivity, and sawtooth-patterned geometries influence busbar temperatures and material usage. A hybrid electrothermal framework, implemented in the InterConX2D simulation environment, is employed to perform detailed analyses of electrical-thermal interactions. The findings are experimentally validated, and the results offer actionable guidelines for engineers seeking to design cost-effective, compact, and thermally optimized busbar systems.

2 Electrothermal Modelling

2.1 Electromagnetic Model - PEEC

Accurate characterization of busbar losses requires detailed modeling of electromagnetic behavior, particularly under high-current conditions where skin and proximity effects are prominent. In this study, the Partial Element Equivalent Circuit (PEEC) method is employed in the frequency domain to transform Maxwell's equations into a network of partial inductances, mutual couplings, and resistances distributed over volumetric cells. This approach provides a full-wave, yet computationally efficient, representation of current distribution and inductive coupling within the busbar structure. Unlike conventional lumped models, the detailed PEEC formulation [4]–[6] captures non-uniform current densities arising from geometric configurations and neighboring conductor interactions. Resistive losses are locally evaluated as a function of current density and frequency-dependent material properties, enabling precise mapping of Joule heating. This loss distribution then serves as the input to the coupled thermal model, ensuring a strong electrothermal interaction. By adopting this method, the study achieves high-fidelity predictions of thermal behavior while maintaining computational efficiency, supporting the optimization of compact and thermally-constrained busbar systems.

Figure 1 and Figure 2 respectively illustrate the decomposition of the busbar into elementary subconductors and the associated Kirchhoff-like network representing the first discretization layer of the geometry. Based on this representation, the matrix formulation of the equivalent frequency-dependent circuit is established, as shown in Equation (1). The corresponding Joule losses are subsequently evaluated using Equation (2).

$$\begin{bmatrix} v \\ v \\ v \\ v \\ v \end{bmatrix} = \begin{bmatrix} R_1 & 0 & 0 & 0 & 0 \\ 0 & R_2 & 0 & 0 & 0 \\ & & R_3 & 0 & 0 \\ & & & R_4 & 0 \\ & & & & R_5 \end{bmatrix} + \begin{bmatrix} L_{11} & L_{12} & L_{13} & L_{14} & L_{15} \\ L_{21} & L_{22} & L_{23} & L_{24} & L_{25} \\ & & L_{33} & L_{34} & L_{35} \\ & & & L_{44} & L_{45} \\ & & & & L_{55} \end{bmatrix} \cdot j\omega \cdot \begin{bmatrix} i_1 \\ i_2 \\ i_3 \\ i_4 \\ i_5 \end{bmatrix} \quad (1)$$

$$P_{Joule} = \frac{\rho_{rcu}(T) \cdot L_{busbar}}{S_i} \cdot \sum_{j=1}^n i_j^2 \quad (2)$$

where $\rho_{rcu}(T) = \rho_0 \cdot (1 + \alpha \cdot (T - T_0))$ denotes the temperature-dependent resistivity of the busbar material [$m \cdot \Omega$], S_i is the cross-sectional area of the i^{th} sub-conductor [m^2] factored out under the assumption of a uniform mesh, and L_{busbar} represents the total length of the busbar [m].

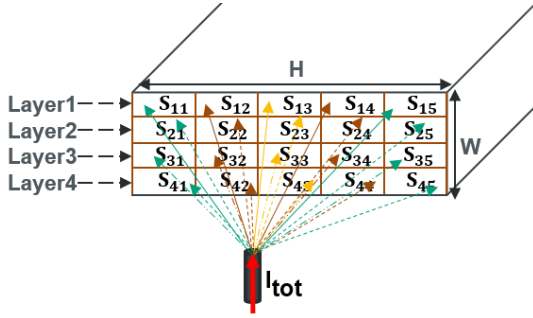


Figure 1: Decomposition of a busbar into sub-conductors.

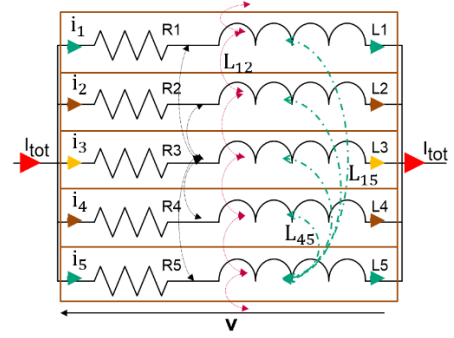


Figure 2: Simplified representation of the busbar's first layer using discrete elements.

2.2 Thermal model

As electric current flows through the conductor, it generates heat due to Joule heating. The busbar must dissipate this heat efficiently to avoid excessive temperature rise that could degrade material properties, compromise insulation, or cause system failure. Consequently, the cross-sectional dimensions of the busbar are selected not only based on electrical requirements but also considering the busbar's thermal dissipation capability. This thermal behavior is described by the general heat transfer Equation (3).

$$\rho_{Cu} C_{pCu} \frac{\partial T}{\partial t} = k_{Cu} \left(\frac{\partial^2 T}{\partial x^2} + \frac{\partial^2 T}{\partial y^2} + \frac{\partial^2 T}{\partial z^2} \right) - \rho_{Cu} C_{pCu} \mathbf{u} \cdot \nabla T + P_{Joule} - P_{Conv} - P_{Rad} \quad (3)$$

where ρ_{Cu} is the material density [kg/m³], C_{pCu} is the specific heat capacity [J/(kg·K)], T is the temperature [K], k_{Cu} is the thermal conductivity [W/(m·K)], \mathbf{u} is the fluid velocity vector (m/s), P_{Joule} is the volumetric heat generation from electrical current [W/m³] and P_{Conv} and P_{Rad} are the power losses via convection and radiation [W/m³].

If convection and radiation are treated via surface boundary conditions (as in most simulation frameworks), then:

* The terms P_{Conv} and P_{Rad} are excluded from the Partial Differential Equation (PDE).

* Instead, they are implemented as convective boundary condition $[-k_{Cu} \nabla T \cdot \mathbf{n} = h(T_{Cu} - T_{\infty})]$ and radiative boundary condition $[-k_{Cu} \nabla T \cdot \mathbf{n} = \epsilon \sigma (T_{Cu}^4 - T_{\infty}^4)]$ where h is convective heat transfer coefficient [W/(m²·K)], T_{∞} the ambient temperature [K], ϵ surface emissivity [-] and σ Stefan-Boltzmann constant (5.67×10^{-8} W/(m²·K⁴)).

Accordingly, Equation (3) simplifies to give Equation (4). This equation is usually coupled with the Navier-Stokes Equations (see Equations (5) and (6)) to model air flow when buoyancy effects are included where variation of fluid density with temperature drives natural convection.

$$\rho_{Cu} C_{pCu} \frac{\partial T}{\partial t} = \nabla \cdot (k_{Cu} \nabla T) - \rho_{Cu} C_{pCu} \mathbf{u} \cdot \nabla T + P_{Joule} \quad (4)$$

* Continuity equation (mass conservation):

$$\nabla \cdot \mathbf{u} = 0 \quad (5)$$

* Momentum equation (incompressible fluid with Boussinesq approximation [7]):

$$\rho_{fl} \left(\frac{\partial \mathbf{u}}{\partial t} + (\mathbf{u} \cdot \nabla) \mathbf{u} \right) + \nabla p - \mu \nabla^2 \mathbf{u} = -\rho_{fl} (T - T_0) \beta \mathbf{g} \quad (6)$$

where p is the pressure [Pa], μ is the dynamic viscosity [Pa·s], ρ_{fl} is the fluid density [kg/m³], \mathbf{g} is the gravity vector [m/s²], β is the thermal expansion coefficient [1/K], and T_0 is the reference temperature [K].

However, in this study, we focus solely on the solid components of the busbar (copper or aluminum core and insulation). The surrounding air domain is not modeled explicitly. Instead, convection and radiation are applied directly at the boundary of the solid, eliminating the need for fluid velocity computation. Consequently, the advective term ($\rho_{Cu} C_{pCu} \mathbf{u} \cdot \nabla T$), which accounts for energy transport due to the bulk motion of fluid within the domain—commonly referred to as volumetric or advective heat transfer—can be neglected in the absence of surrounding fluid flow modeling. Simultaneously, assuming that the busbar reaches thermal equilibrium

rapidly with minimal internal thermal gradients, the conductive diffusion term ($\nabla^2 T$) can also be disregarded. This simplifies the problem to a surface-dominated heat transfer scenario where only net heat gains and losses over the control volume are considered, resulting in a lumped-capacitance model as shown in Equation (7).

$$\rho_{Cu} C_{pCu} \frac{\partial T}{\partial t} = P_{Joule} - P_{Conv} - P_{Rad} \quad (7)$$

Here, P_{Conv} and P_{Rad} represent respectively the total heat loss through the surface due to convection and radiation. Though physically occurring at boundaries, their effects are aggregated and represented as equivalent volumetric losses in the global energy balance as shown in table Table 1.

Table 1: Summary on Equation (7) terms.

| Terms | Physically Occurs At | Descriptions |
|-------------|----------------------|---|
| P_{Joule} | Inside conductor | Internal heating by Joule effects |
| P_{Conv} | Conductor surface | Total power loss based on $hA(T_{Cu} - T_{\infty})$ |
| P_{Rad} | Conductor surface | Total power loss based on $\epsilon\sigma A(T_{Cu}^4 - T_{\infty}^4)$ |

For transient simulations, a two-node thermal model could be used. This model (see in Equations (8) and (9)) captures the thermal behavior by considering discrete nodes connected through thermal resistances and governed by capacitance:

* Node 1 (Copper or Aluminium core):

$$\rho_{Cu} C_{pCu} V_{Cu} \cdot \frac{\partial T_{Cu}}{\partial t} = P_{Joule} - \frac{T_{Cu} - T_{ins}}{R_{ins}} \quad (8)$$

* Node 2 (PVC insulation):

$$\rho_{ins} C_{pins} V_{ins} \cdot \frac{\partial T_{ins}}{\partial t} = P_{Joule} - \frac{T_{Cu} - T_{ins}}{R_{ins}} - hA(T_{ins} - T_{\infty}) - \epsilon\sigma A(T_{ins}^4 - T_{\infty}^4) \quad (9)$$

In steady-state where the term $\partial T_{ins}/\partial t$ is equal to zero, a simple thermal resistance method can be used to directly determine the copper core temperature once the PVC surface temperature is known as shown in Equation (10).

$$T_{Cu} = T_{ins} + P_{Joule} \cdot \frac{e_{ins}}{(k_{ins} \cdot P_{ins} \cdot L_{busbar})} \quad (10)$$

with $e_{ins}/(k_{ins} \cdot P_{ins} \cdot L_{busbar})$ is the thermal resistance of the insulation material, where P_{ins} represents its perimeter [m].

This highlights that the resistance determines how efficiently heat is transferred from the copper core to the environment. Therefore, in the next section, geometric and material parameters of the busbar surface and insulation will be explored to optimize thermal performance. Hence, it is essential to introduce the dimensionless numbers employed to evaluate the convective heat transfer coefficient, as referenced in Equation (13). In the case of natural convection around a vertically oriented busbar, the convective heat transfer is typically characterized using the Nusselt number (Nu), which quantifies the enhancement of heat transfer due to convection relative to pure conduction. For such configurations, the Nusselt number is commonly correlated as a function of the Rayleigh number (Ra), which is defined as the product of the Grashof number (Gr) and the Prandtl number (Pr). Specifically, for a vertical surface, the Rayleigh number is given by Equation (11):

$$Ra(T_s) = Gr(T_s) \cdot Pr(T_s) = \frac{g\beta(T_s - T_{\infty})L_c^3}{\vartheta^2} \cdot \frac{\vartheta}{\alpha} = \frac{g\beta(T_s - T_{\infty})L_c^3}{\vartheta\alpha} \quad (11)$$

Where β is the thermal expansion coefficient [1/K], T_s is the surface temperature [K], L_c is the characteristic length (typically vertical height) [m], ϑ is kinematic viscosity [m²/s], and α is thermal diffusivity [m²/s].

The Grashof number represents the ratio of buoyancy to viscous forces, while the Prandtl number describes

the ratio of momentum diffusivity to thermal diffusivity. The Rayleigh number, therefore, governs the onset and strength of natural convection flow.

For vertical surfaces subject to natural convection, one of the most reliable empirical correlations for the Nusselt number is provided in [8] by Churchill and Chu. This correlation is applicable over a wide Rayleigh number range and accounts for both laminar and turbulent boundary layer behaviors:

$$Nu(T) = \left\{ 0.825 + \frac{0.387(R_a(T))^{1/6}}{[1 + ((0.492/P_r(T))^{9/16})^{8/27}]^{1/4}} \right\}^2 \quad (12)$$

These dimensionless parameters are essential for selecting or deriving empirical correlations for the Nusselt number $Nu = f(R_a, P_r)$ which in turn determines the convective heat transfer coefficient h via:

$$h(T) = \frac{Nu(T_s) \cdot \lambda_d(T_s)}{L_c} \quad (13)$$

where λ_d is the thermal conductivity of the fluid [W/(m·K)]

This framework provides a robust and generalized approach to estimate h , enabling more accurate evaluation of the convective losses $P_{conv} = hA(T_s - T_\infty)$ introduced earlier in Equation (9).

2.2.1 Surface state of the busbars

The surface condition of a busbar plays a critical role in its thermal performance, particularly in how effectively it dissipates heat through convection and radiation. Reducing the cross-sectional area of the conductor while maintaining the same current-carrying capacity leads to an increase in power density (i.e., Joule losses per unit volume), thereby elevating internal heat generation. Consequently, enhancing surface heat dissipation becomes essential to maintain operating temperatures within safe limits.

In the following subsections, we distinguish between non-insulated and insulated busbars, examining the thermal implications of their surface treatments. For both configurations, enhancements can be linked back to the lumped thermal model in Equation (7), by adjusting the values of P_{conv} and P_{rad} .

2.2.2 Non-insulated busbars

The enhancement of emissivity through the application of coatings (e.g., black anodising, oxide layers) results in a transformation of the surface from a poor radiator ($\varepsilon \approx 0.05 - 0.1$) to an efficient emitter ($\varepsilon \approx 0.7 - 0.95$). This has a substantial impact on the P_{rad} parameter within the energy balance model. For more accurate modeling, the use of temperature-dependent emissivity functions, $\varepsilon(T)$, is recommended over constant values. These functions, detailed in Equations (14) and (15), describe emissivity behavior for highly polished and stably oxidized copper, respectively, and are illustrated in Figure 3 and Figure 4. To better reflect gradual physical phenomena such as oxide growth, surface aging, or phase transitions, a linear interpolation is adopted, ensuring smooth transitions in $\varepsilon(T)$ rather than abrupt changes.

Additionally, surface roughness (rugosity) plays a dual role in thermal performance. In addition to enhancing emissivity, increased roughness modifies convective heat transfer by disrupting boundary layer flow, thereby promoting localized turbulence. This can raise the Nusselt number and improve the overall convective cooling capacity of the busbar.

$$\varepsilon(T) = \varepsilon_i + \frac{(T - T_i)(\varepsilon_{i+1} - \varepsilon_i)}{(T_{i+1} - T_i)}, \text{ for } T \in [T_i, T_{i+1}] \quad (14)$$

where $T_i = [100 \ 200 \ 400 \ 600 \ 800 \ 1000 \ 1200 \ 1400 \ 1500] - 273.15$ °C and $\varepsilon_i = [0.02 \ 0.02 \ 0.03 \ 0.03 \ 0.04 \ 0.04 \ 0.05 \ 0.05 \ 0.06]$

$$\varepsilon(T) = \begin{cases} 0.4, & \text{if } T \leq 300 \text{ °C} \\ 0.6706 + -1.094e^{-3}T + 1.75e^{-6}T^2, & \text{if } T > 300 \text{ °C} \end{cases} \quad (15)$$

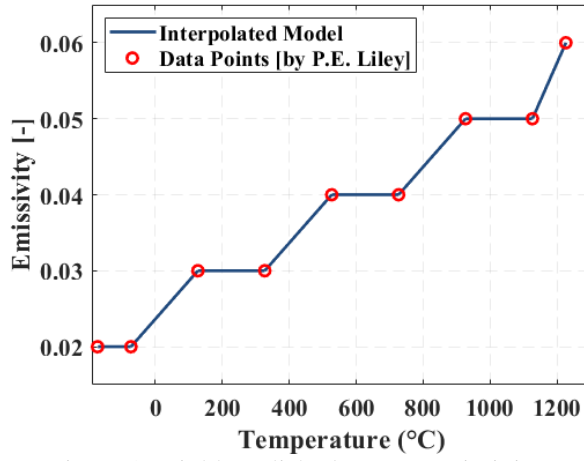


Figure 3: Highly polished copper emissivity vs temperature.

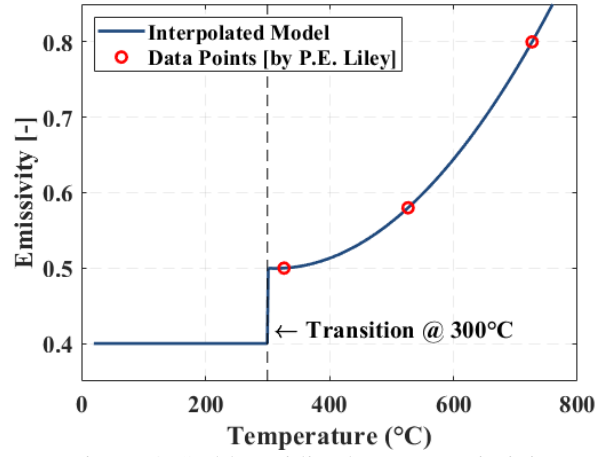


Figure 4: Stably oxidized copper emissivity vs temperature.

2.2.3 Insulated busbars

In insulated configurations, both the thermal conductivity and geometry of the insulating layer must be optimized to minimize thermal resistance while enabling surface-level cooling. The insulation layer introduces an additional resistance, which directly influences heat flow from the copper (or aluminum) core to the ambient environment. According to the energy balance equation extended for the insulation node in Equation (9) color modification of the insulation can significantly enhance emissivity, while careful selection of insulation thickness balances protection with thermal efficiency. Excessive thickness increases thermal resistance and can suppress convective cooling by insulating the surface from airflow.

Moreover, sawtooth patterning of the outer insulation surface (see Figure 5) serves two key functions: increasing the effective radiating surface area and promoting vortex formation which increases convective efficiency. These effects can be integrated into the model by adjusting surface area A (see Equation (16)), and the convection coefficient h via modified empirical Nusselt number correlations.

$$A = A_{top,bottom} + A_{label} + A_{radius} + A_{sawtooth} \quad (16)$$

where $A_{top,bottom} = (W + 2 \cdot e_{ins1}) \cdot L_{busbar} \cdot 2$, $A_{label} = H_{label} \cdot L_{busbar}$

$$A_{radius} = R \cdot \theta_{ins} \cdot \left(\left[\frac{2 \cdot H - H_{label}}{d_{ins}} \right] \right) \cdot L_{busbar} \cdot 2, \quad A_{sawtooth} = \frac{e_{ins2}}{\cos(\theta_{ins}/2)} \cdot \left(\left[\frac{2 \cdot H - H_{label}}{d_{ins}} \right] \right) \cdot L_{busbar} \cdot 2$$

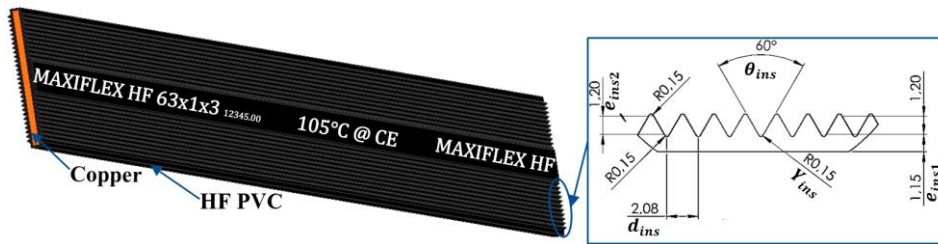


Figure 5: Sawtooth-patterned HF PVC insulator.

with e_{ins1} is the base insulation thickness [mm], e_{ins2} is the sawtooth length from base to peak [mm], d_{ins} is the tooth pitch (peak to peak) [mm], θ_{ins} is the tooth angle [degrees/in radians for A_{radius} calculation], H_{label} is the flat zone reserved for label per lateral face [mm], R is the Radius of the tooth tip [mm], H is the Height of the busbar [mm], and W is the Thickness of the busbar [mm].

This formulation captures the increase in surface area due to the inclined faces of the sawtooth structure, modeled through the geometric correction factor. The total number of teeth along the height is approximated using a floor function, and the added contribution from the side surfaces is also included. This approach enables a consistent comparison with the base case while integrating the geometric enhancement into the thermal balance.

To validate and quantify these surface enhancement strategies, in the next section, the effect of emissivity, insulation geometry, and sawtooth patterning on steady-state temperatures under equivalent electrical loading

are evaluated. Output results will support the thermal model refinements discussed and guide the design of more efficient, compact busbars.

3 Results and discussion

3.1 Quantification of Electrothermal Coupling Effects: Impact of Surface Emissivity

In this section, we aim to quantitatively evaluate the influence of surface emissivity on the thermal behavior of the busbar, while also assessing the impact of electrothermal coupling—i.e., the feedback effect between temperature rise and electrical resistivity. To do so, we consider multiple simulation scenarios where the emissivity of the copper surface is varied from low (highly polished) to high (oxidized or coated), and the electrical resistivity is either kept constant or allowed to evolve with temperature. This approach allows us to decouple the pure radiative effects from the coupled electrothermal phenomena, and to assess their respective contributions to the overall temperature rise and power dissipation of the system.

The busbar used in this study has a height (H) of 63 mm, a width (W) of 3 mm, and a length (L_{busbar}) of 1300 mm, and is subjected to a current of 876 A at 50 Hz. Note that the simulations presented in these sections were performed using the InterConX2D simulation environment.

Table 2: Effect of emissivity on thermal performance.

| Inputs | Cases | Coupling | $\rho_{rcu}(^{\circ}\text{C})$ | Emissivity | $T_{Cu}(^{\circ}\text{C})$ |
|--|-------|----------|--------------------------------|-------------|----------------------------|
| $T_{amb} = 23^{\circ}\text{C}$ $h = 7 \text{ W/m}^2 \cdot \text{K}$ | 1 | No | $\rho_{rcu}(23)$ | 0.1 | 90.8 |
| | 2 | No | $\rho_{rcu}(23)$ | 0.95 | 61.5 |
| | 3 | Yes | $\rho_{rcu}(T_{Cu})$ | 0.1 | 104.8 |
| | 4 | Yes | $\rho_{rcu}(T_{Cu})$ | 0.95 | 68.2 |

Obtain results in the Table 2 show how coupling modifies the thermal state and highlight the nonlinear interaction between electrical and thermal phenomena. It is important to note that heat transfer coefficient h is considered constant only in the case 1 and 2. It should be emphasized that the temperature variations observed are qualitatively consistent with expected physical behavior.

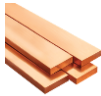

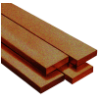

3.1.1 Impact of surface treatments on Non-insulated busbars

This investigation evaluates surface treatment strategies to optimize convective and radiative heat transfer in non-insulated busbar systems. The study systematically examines two distinct approaches:

- **Controlled Microstructure Fabrication : Surface Roughness Effect**

Deliberate modification of surface roughness is achieved through chemical oxidation processes, aiming to disrupt the formation of the thermal boundary layer and enhance the emissivity of the Busbar material. This method increases thermal radiation exchange efficiency. The applied oxidation process produces an organometallic layer with a thickness of a few microns, featuring a carefully engineered surface topography. This layer not only serves as a protective barrier but also significantly increases radiative emissivity by altering the optical and thermal properties of the treated surface. Table 3 presents the temperature of a $63 \times 3 \text{ mm}^2$ busbar for different levels of surface roughness (R_a).

Table 3: Roughness Effect on busbar temperature.

| | Smooth Surface | $R_a = 0.23 \mu\text{m}$ | $R_a = 0.58 \mu\text{m}$ | $R_a = 0.96 \mu\text{m}$ |
|--------------------------------|---|---|--|---|
| Cases |  |  |  |  |
| $T_{amb} = 23^{\circ}\text{C}$ | | | | |
| Temperatures | 96.70 $^{\circ}\text{C}$ | 90.4 $^{\circ}\text{C}$ | 81.1 $^{\circ}\text{C}$ | 73.3 $^{\circ}\text{C}$ |
| Emissivity | 0.2 | 0.3 | 0.5 | 0.74 |

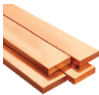
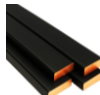
The increase in surface roughness enhances thermal emissivity by reducing reflectivity and promoting multiple internal reflections of incident radiation. Rough textures increase the chances of infrared absorption by scattering light, allowing it to interact with the surface multiple times. As a result, absorption rises and, per

Kirchhoff’s law, so does emissivity—since a surface that absorbs more also emits more. Smooth surfaces, by contrast, reflect more light and absorb less, leading to lower emissivity. Thus, increasing roughness supports better radiative heat dissipation.

• **Surface Coating Application: High-Emissivity Painting Effect**

Surface painting modifies the optical properties of the busbar by significantly increasing its emissivity, especially in the infrared spectrum. This method is particularly attractive due to its simplicity, cost-effectiveness, and adaptability to existing systems. The following results highlight the impact of different surface finishes and paint types on busbar temperature and emissivity. It assumed that the paint layer is unifom with thermal conductivity of 1.5 W/(m·K) with an emissivity of 0.95.

Table 4: Painting Effect on busbar temperature.

| | Uncoated | Paint Layer Thickness (e_{th}) | | |
|---------------------------------|---|--|------------------|------------------|
| | Surface | 20 μm | 60 μm | 100 μm |
| Cases |  |  | | |
| $T_{amb} = 23\text{ }^{\circ}C$ | | | | |
| Temperatures | 96.70 $^{\circ}C$ | 68.3 $^{\circ}C$ | 68.2 $^{\circ}C$ | 68.1 $^{\circ}C$ |
| Emissivity | 0.2 | 0.95 | 0.95 | 0.95 |

Thin thermal coatings (20–100 μm) introduce minimal thermal resistance due to their negligible thickness relative to the overall thermal path of the busbar system. Consequently, the variation in surface temperature—from 68.3 $^{\circ}C$ to 68.1 $^{\circ}C$ across increasing thicknesses—is marginal. In this range, the slight increase in thickness may actually stabilize emissivity by ensuring more uniform coverage and a smoother surface finish, which enhances the effective emissivity in real-world conditions. Overall, the dominant factor driving the observed temperature drop is the significant improvement in emissivity.

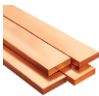
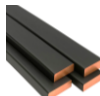
3.1.2 **Impact of Insulators on Insulated Busbars**

This section evaluates how different insulator characteristics affect the thermal behavior of insulated busbars. Key parameters include the thickness of the insulation layer, its thermal conductivity, and the influence of surface geometry modifications such as sawtooth patterning—all of which directly impact heat dissipation external convection/radiation.

• **Insulator Thickness Effect (1 to 2mm)**

Varying the thickness of the insulation layer influences the total thermal resistance between the copper conductor and the ambient environment. This part explores how slight increases in thickness (within practical ranges) affect surface temperatures and heat rejection efficiency. Here, the thermal conductivity of considered insulator is 0.18W/(m·K) with an emissivity of 0.92.

Table 5: Insulator thickness effet on busbar temperature.

| | Non-insulated Busbar | Insulator Thickness (e_{ins}) | | |
|---------------------------------|---|--|------------------|------------------|
| | | 1 mm | 1.5 mm | 2 mm |
| $T_{amb} = 23\text{ }^{\circ}C$ |  |  | | |
| T_{Cu} (Copper) | | | | |
| | 96.76 $^{\circ}C$ | 70.6 $^{\circ}C$ | 71.5 $^{\circ}C$ | 72.5 $^{\circ}C$ |
| T_{ins} (Insulator) | | 67.1 $^{\circ}C$ | 66.2 $^{\circ}C$ | 65.5 $^{\circ}C$ |
| Emissivity | 0.2 | 0.92 | 0.92 | 0.92 |

Surface coating with high-emissivity, thermally conductive paint demonstrates that modest increases in thickness can serve as thermal buffers, slightly stabilizing temperature fluctuations while enhancing radiative dissipation. In contrast, when using insulating materials with low thermal conductivity,

increasing thickness into the millimeter range significantly raises the thermal resistance. This hinders heat transfer from the copper core to the environment, resulting in higher surface temperatures and reduced cooling efficiency.

• Insulator's Thermal Conductivity Effect (0.15 – 0.30 W/(m·K))

The thermal conductivity of the insulating material dictates how efficiently heat is transmitted through the insulation. This subsection analyzes how choosing materials with different conductivities alters the temperature distribution across the busbar. Figure 6 illustrates the variation of the copper and insulator surface temperatures as a function of insulator thickness for several thermal conductivities. Figure 7, on the other hand, presents the evolution of these temperatures with varying insulator thickness for each fixed thermal conductivity value.

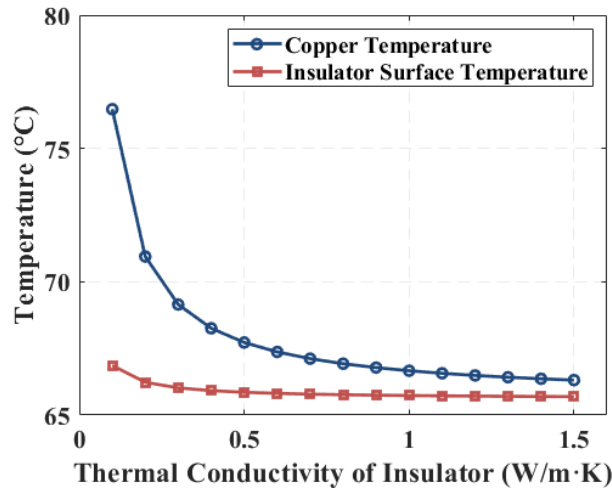


Figure 6: Surface temperatures vs. thermal conductivities for 1.5mm insulator thickness.

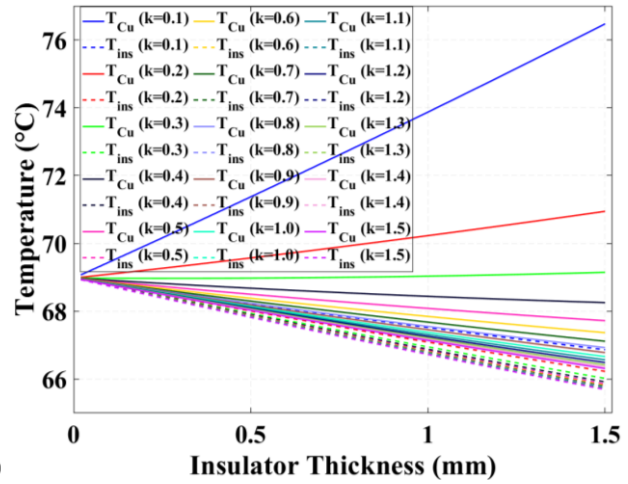


Figure 7: Surface temperatures vs. insulator thickness for each thermal conductivity value.

The plot shows that as the thermal conductivity of the insulation material increases (from 0.1 to 2.0 W/(m·K)), both the copper surface temperature and the outer insulator surface temperature steadily decrease. This is because a higher thermal conductivity facilitates more efficient heat transfer through the insulation, allowing the heat generated in the copper conductor to be dissipated more effectively to the environment.

At low conductivities (e.g., 0.1 W/(m·K)), the insulation behaves more like a thermal barrier, trapping heat and raising the internal copper temperature (up to 76.5 °C). As conductivity increases, this barrier effect diminishes, resulting in a sharp drop in copper temperature initially, which then gradually stabilizes around 66 °C. The insulator surface temperature, which governs the radiative cooling, also benefits from improved conductivity, achieving slightly lower values with increasing conductivity, though the change becomes marginal past 1.0 W/(m·K). Overall, improving thermal conductivity of the insulating layer significantly enhances thermal dissipation and keeps both the busbar and its surface cooler.

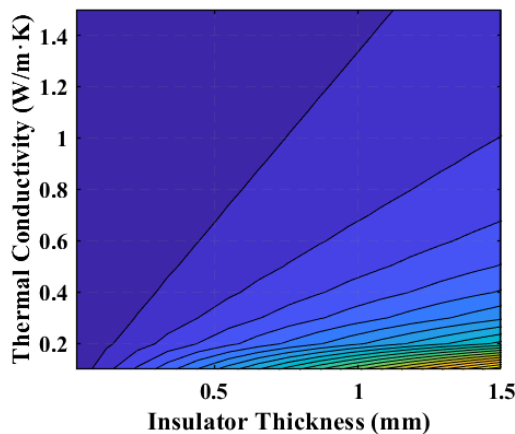


Figure 8: Surface temperatures difference ($\Delta T = T_{Cu} - T_{ins}$).

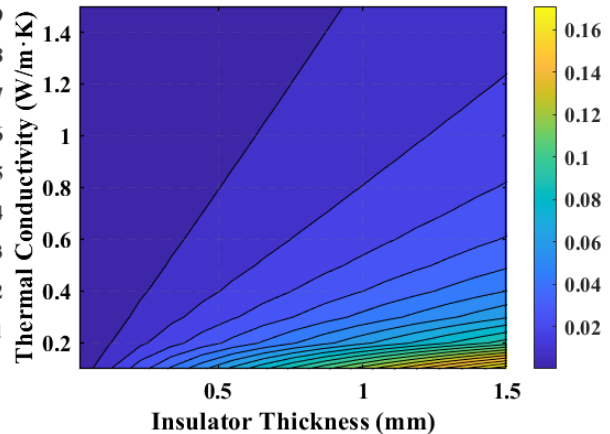


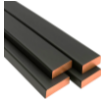

Figure 9: Thermal efficiency of insulator ($\eta = (T_{Cu} - T_{ins}) / (T_{Cu} - T_{amb})$).

The thermal behavior of the busbar system reveals two dominant trends: temperatures decrease with increasing thermal conductivity and increase with insulation thickness. For a fixed thickness, both the copper (T_{cu}) and surface insulator (T_{ins}) temperatures decline as conductivity rises, reflecting improved heat dissipation. Conversely, thicker insulation degrades thermal transfer, reducing heat loss and causing internal temperatures to rise. At constant conductivity, this results in a noticeable increase in T_{cu} with thickness. Higher conductivity at fixed thickness leads to elevated T_{ins} values, indicating a more efficient heat transfer to the environment. A saturation effect is observed at low conductivities and large thicknesses, where T_{cu} stabilizes—suggesting nearly adiabatic conditions. The performance of the insulation, evaluated by the temperature difference $\Delta T = T_{cu} - T_{ins}$ (see Figure 8), peaks for conductivities below $0.4 \text{ W}/(\text{m}\cdot\text{K})$ and thicknesses above 1 mm , highlighting optimal configurations. Lastly, thermal efficiency—defined here in relative terms—decreases with increasing conductivity, while a plateau is reached under conditions of low conductivity and large thickness, indicating effective thermal confinement within the system (Figure 9). Nevertheless, the primary function of the insulating layer remains electrical safety, and its dielectric strength must also be considered in material selection.

- **Sawtooth Patterned Effect**

Applying a sawtooth pattern on the insulation's outer surface modifies both convective and radiative heat transfer. This part investigates how these geometrical changes affect the effective surface area, aiming to enhance overall thermal dissipation. It is important to note that the addition of the sawtooth pattern does not impact the characteristic length of the vertical busbar. Therefore, the characteristic length remains defined as $H + 2 \cdot e_{ins1}$, corresponding to the total physical height of the surface exposed to the flow. This is because the height of the object facing gravity is what primarily governs buoyancy-driven (natural convection) behavior, not the increased surface contour introduced by the sawtooth profile. The results obtained for the standard flat-surface busbar and the sawtooth-patterned busbar are presented in the table below.

Table 6: Sawtooth patterned effect on busbar temperature.

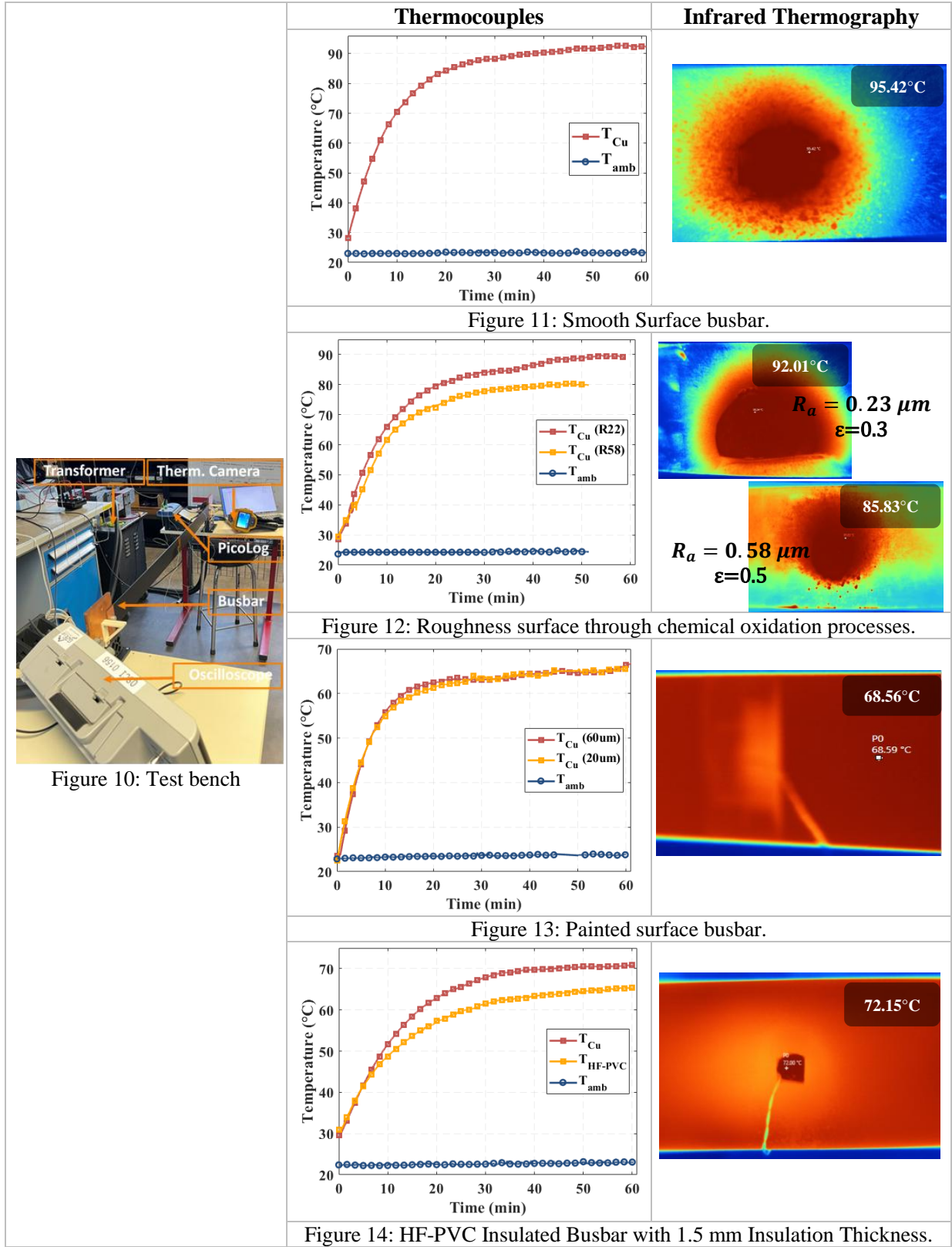
| | Flat-surface | Sawtooth Angle (θ_{ins}) | | |
|---|---|-----------------------------------|--|-------------------------|
| | busbar | 30° | 45° | 60° |
| $T_{amb} = 23 \text{ }^{\circ}\text{C}$ |  | |  | |
| T_{Cu} (Copper) | 71.1 $^{\circ}\text{C}$ | 64.7 $^{\circ}\text{C}$ | 62.1 $^{\circ}\text{C}$ | 59.3 $^{\circ}\text{C}$ |
| T_{ins} (Insulator) | 65.8 $^{\circ}\text{C}$ | 58.7 $^{\circ}\text{C}$ | 56.1 $^{\circ}\text{C}$ | 53.4 $^{\circ}\text{C}$ |
| Emissivity | 0.92 | 0.92 | 0.92 | 0.92 |

The results clearly show that applying a sawtooth pattern on the insulation surface significantly improves the thermal behavior of the busbar. Compared to the flat-surface case, the addition of sawtooth patterns leads to a noticeable decrease in both copper and insulator temperatures. Furthermore, the cooling effect becomes more pronounced as the sawtooth angle increases: at 30° , the copper temperature drops by approximately 6.4°C compared to the flat case, while at 60° , the temperature reduction reaches around 11.8°C . This progressive improvement is mainly attributed to the increase in effective surface area and the generation of localized turbulence, which together enhance convective and radiative heat transfer. Since the emissivity remains constant across all configurations, the observed benefits are purely due to geometric surface modification rather than changes in material properties. Overall, the sawtooth pattern demonstrates strong potential for passive cooling enhancement.

3.2 Experimental results

An experimental test bench was constructed to validate the numerical results discussed in the preceding sections (Figure 10). Temperature measurements were carried out using two complementary techniques: thermocouples strategically placed on the busbar surface and infrared thermography via a thermal camera (Figure 10). Obtained results are shown from Figure 11 to Figure 14.

Table 7: Validation of busbar thermal behavior.



Experimental validation confirms the model's accuracy, demonstrating that the proposed hybrid approach enables rapid, cost-effective, and computationally efficient analysis for busbar design optimization.

4 Conclusion

This study has systematically evaluated multiple strategies for optimizing material usage in electrical systems through thermal management, addressing the growing demand for more compact, sustainable, and high-performance busbar designs. Moving beyond conventional sizing rules and standard finite element techniques, a hybrid electrothermal modeling framework coupling the Partial Element Equivalent Circuit (PEEC) method with thermal energy balance equations was employed to enable rapid and accurate parametric exploration of surface and insulation design strategies.

Key insights include:

- **Surface Roughness & Emissivity:** Increasing roughness (R_a up to $0.96\ \mu\text{m}$) reduced busbar temperature from $96.7\ ^\circ\text{C}$ to $73.3\ ^\circ\text{C}$ due to increased emissivity (from 0.28 to 0.74), confirming radiation as the dominant mechanism. This enables up to 24% temperature reduction without enlarging conductor size.
- **High-Emissivity Coatings:** Coatings with $\varepsilon = 0.95$ yielded a 32% surface temperature decrease compared to $\varepsilon = 0.1$, despite a slight rise in thermal resistance highlighting their effectiveness in stabilizing thermal transients.
- **Sawtooth-Patterned Geometries:** Simulations showed a 22% to 45% increase in surface area, lowering busbar temperature by up to $12\ ^\circ\text{C}$. Ongoing experimental work aims to precisely characterize the optimal geometry of the sawtooth angle for maximizing heat rejection.
- **Insulation Properties:** The joint effect of insulation thickness and thermal conductivity was shown to be nonlinear, with an identifiable optimal region that balances thermal performance with dielectric safety.

Altogether, these strategies enable a potential reduction of up to 41% in busbar cross-sectional area translating into significant material savings while maintaining thermal and electrical reliability. The hybrid methodology developed here provides engineers with a computationally efficient yet physically rigorous tool for the design of resource-optimized busbars.

Future work will address more complex installations—such as mobile systems and enclosed switchgear—where enclosure-induced multiphysics effects significantly impact current and thermal distributions.

References

- [1] Danesh Daroui, *Implementation and optimization of partial element equivalent circuit-based solver*. Luleå, 2010.
- [2] P. Holman, *Heat Transfer*, 10th ed., McGraw-Hill, 2010.
- [3] *Electrical: Busbar - Table 4: Effect of Emissivity*. [Online]. Available: https://copper.org/applications/electrical/busbar/bus_table4.php. [Accessed: 27 Apr. 2025].
- [4] A. E. Ruehli, *Inductance Calculations in a Complex Integrated Circuit Environment*, IBM Journal of Research and Development, vol. 16, no. 5, pp. 470–481, Sep. 1972.
- [5] A.E. Ruehli and P.A. Brennan, *Efficient Capacitance Calculations for Three-Dimensional Multiconductor Systems*, IEEE Transactions on Microwave Theory and Techniques, vol. 21, no. 2, pp. 76–82, Feb. 1973.
- [6] A.E. Ruehli, *Equivalent Circuit Models for Three-Dimensional Multiconductor Systems*, IEEE Transactions on Microwave Theory and Techniques, vol. 22, no. 3, pp. 216–221, Mar. 1974.
- [7] Christine Bernardi et al., *Couplage des équations de Navier-Stokes et de la chaleur : le modèle et son approximation par éléments finis*, ESAIM: M2AN, vol. 29, no. 7, pp. 871–921, 1995.
- [8] Frank P. Incropera et al., Eds., *Fundamentals of heat and mass transfer*, 6. ed. Hoboken, NJ: Wiley, 2007.

Presenter Biography



Appolinaire E. Dantondji (*1992) studied Electrical and Electronics Engineering at Pamukkale University, Turkey, earning his Dipl.-Ing. degree. He later completed an M.Sc. in Electrical Systems for Energy and Mobility at Paris-Saclay University, France. Currently, he is pursuing a Ph.D. at the University of Grenoble Alpes, France, focusing on developing power conductor sizing approaches with respect to future power system resource constraints.